Cold collisions between argon atoms and hydrogen molecules

J. C. Flasher and R. C. Forrey
Pennsylvania State University, Berks-Lehigh Valley College, Reading, Pennsylvania 19610-6009
(Received 17 July 2001; published 13 February 2002)

Collisions between argon atoms and hydrogen molecules are investigated at very low temperatures. Quantum-mechanical calculations are performed using two different potential-energy surfaces. Rate coefficients for all possible combinations of initial vibrational and rotational level have been computed in the limit of zero temperature. Resonant and quasiresonant behavior is found using both potential-energy surfaces. The results are interpreted and estimates are made of the reliability of the calculations.

DOI: 10.1103/PhysRevA.65.032710 PACS number(s): 34.50.Ez, 34.10.+x

I. INTRODUCTION

In a series of recent papers [1–5], various aspects of rovibrational energy transfer in ultracold atom-diatom collisions were explored. Motivated by experimental methods such as helium buffer gas cooling [6] and helium cluster isolation spectroscopy [7], the theoretical studies each assumed a helium atom collision partner. The helium experiments, together with other cooling and trapping schemes [8–16], have opened up a new temperature regime to study atom-molecule dynamics. Most of the current experiments involving cold molecules involve atoms that are heavier and interact more strongly than helium. Therefore, it is desirable to extend the investigations [1–5] to include atoms that are heavier and allow a deeper van der Waals potential well than systems that contain helium atoms.

It is also generally desirable to provide estimates of the accuracy of the calculations. Because potential-energy surfaces are not designed for ultracold temperatures, it is difficult to estimate the accuracy of results that employ them. It was shown [1] that the cross section for exothemic vibrational relaxation in ultracold He-H_2 collisions decreased by several orders of magnitude when the long-range part of the potential was neglected. More realistic estimates of the accuracy of the scattering results may be made when there exists more than one reliable parametrization of the potential-energy surface for a given system. Such is the case for Ar-H_2 where we have employed the use of both parametrizations reported by Schwenke, Walch, and Taylor [17].

New techniques have been developed recently for preparing molecules in highly excited vibrational and rotational states [18,19]. Techniques based on photoassociation spectroscopy typically produce vibrationally excited molecules as intermediate states [8–12]. In many experiments involving ultracold molecules, it is the total collisional relaxation [2] that is important. In these cases, it is sufficient to describe the collisions in terms of a complex scattering length [20]. The imaginary part of the scattering length is proportional to the total zero-temperature quenching rate coefficient. This may be found by solving a set of coupled-channel equations and summing all state-to-state rate coefficients that are connected to the incoming channel. However, if it is only the total rate coefficient that is desired, then it should be possible to model the interaction using a radially symmetric complex optical potential. In the present work, we begin to address this issue by considering a complex square-well potential. We demonstrate that many of the important features of a numerically exact coupled-channel calculation may be qualitatively understood in terms of this simple model.

With the aid of the complex scattering length, a kinetic model may be constructed for describing the relaxation of vibrationally or rotationally excited trapped molecules [2]. The relaxation may be due to direct collisional quenching or to the formation and decay of van der Waals complexes. When the end-over-end angular momentum of the complex is zero and the vibrational stretching quantum number is the largest possible integer that allows the complex to be bound, it is possible to use effective range theory to compute the lifetimes for predissociation [2,21]. The numerical tests that confirmed the reliability of the effective range theory were performed on $He\cdots H_2$ that supported only a single bound state. In the present work, we perform similar tests for $Ar\cdots H_2$ where several bound states exist.

It was previously demonstrated [21] that predissociation of the most weakly bound state of a van der Waals complex is influenced by the same quasiresonant vibration-rotation energy transfer that is found in atom-diatom collisions [22]. It was also shown that the proximity of closed quasiresonant channel thresholds provides a strong influence on the lifetimes [21]. In the present work, we study the analytic structure of the threshold behavior obtained using both parametrizations of the Ar-H_2 potential-energy surface and investigate whether quasiresonant dynamics has any influence on the more deeply bound states of the complex.

The paper is organized as follows: in Sec. II, we describe a few qualitative features of the potential-energy surface that are important for our investigations. Section III provides a review of the standard close-coupling formalism that we used to obtain an extensive database of rovibrational rate coefficients and predissociation lifetimes for both of the parametrized surfaces. In Sec. IV, we demonstrate how a complex square-well potential may be used to provide a qualitative description of several of the key results that are found from the numerically exact coupled-channel calculations. These results are presented in Sec. V. Conclusions to our investigation are given in Sec. VI.

II. POTENTIAL-ENERGY SURFACE

For the Ar-H_2 potential-energy surface, we use both fits reported by Schwenke, Walch, and Taylor [17]. Surface 1

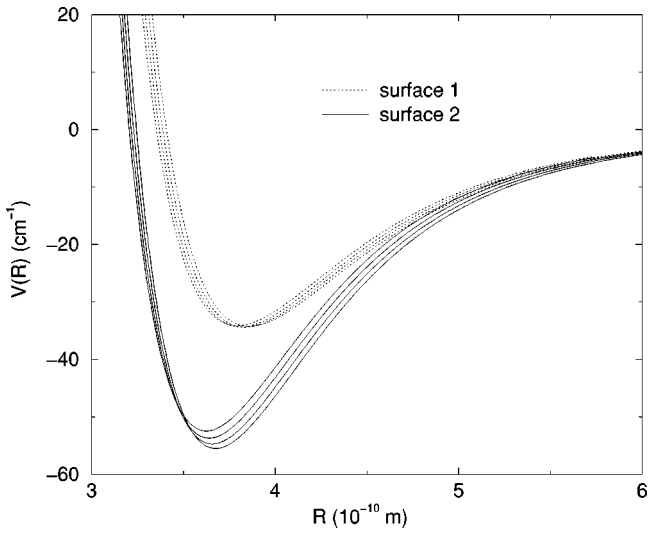

FIG. 1. Spherically symmetric part of the $Ar+H_2$ interaction potential averaged over the vibrational wave function for $v=1,2,3,4$. The well depth differs by about 20 cm^{-1} for the two potential-energy surfaces and does not vary significantly with v.

reproduces *ab initio* data but not empirical estimates of the van der Waals well while surface 2 smoothly interpolates between the *ab initio* data and empirical estimates of the van der Waals well [17]. Figure 1 shows the spherically symmetric part of the $Ar+H_2$ interaction potential averaged over the vibrational wave function for $v=1,2,3,4$. The well depth for the two potential-energy surfaces differ by about 20 cm^{-1} but does not vary significantly with v. Figure 2 shows the spherically symmetric part of the $Ar+H_2$ interaction potential averaged over the vibrational wave function for $v=6,8,10,12$. As the diatomic vibrational energy is increased towards dissociation, the well depth decreases and is pulled outward. Because these fits were designed to be used in energy transfer studies involving dissociation and recombination [17], they can be expected to model the large stretching that is important for vibrational relaxation of highly excited molecules.

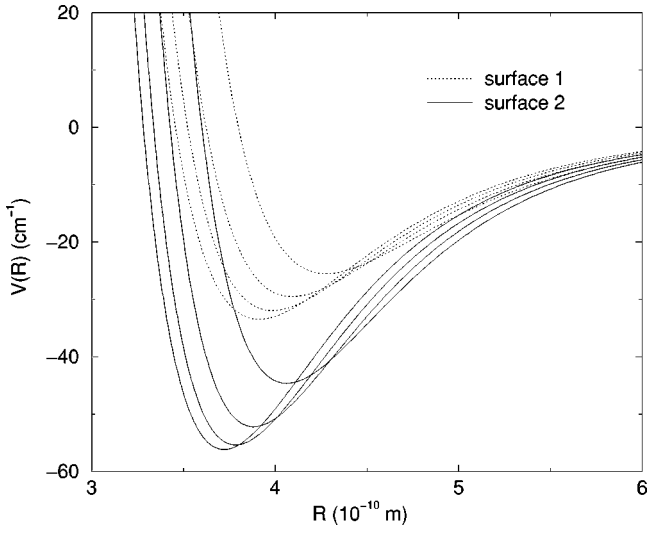

FIG. 2. Spherically symmetric part of the $Ar+H_2$ interaction potential averaged over the vibrational wave function for $v=6,8,10,12$. As the diatomic vibrational energy is increased towards dissociation, the well depth decreases and is pulled outward.

III. CLOSE-COUPLING EQUATIONS

We have computed rate coefficients for all possible combinations of initial vibrational and rotational level in the limit of zero translational temperature. The computations were performed separately for each potential-energy surface using an exact quantum-mechanical close-coupling formulation. For the sake of completeness, we provide a brief review of the diabatic close-coupling procedure used in the present work. The atom-diatom Hamiltonian in the center-of-mass frame is given by

$$H=-\frac{1}{2m}\nabla_r^2-\frac{1}{2\mu}\nabla_R^2+v(r)+V_I(r,R,\theta), \tag{1}$$

where r is the distance between the hydrogen atoms, R is the distance between the argon atom and the center of mass of the diatom, θ is the angle between r and R, m is the reduced mass of the diatom, and μ is the reduced mass of the argon atom with respect to the diatom.

The diatomic Schrödinger equation

$$\left[\frac{1}{2m}\frac{d^2}{dr^2}-\frac{j(j+1)}{2mr^2}-v(r)+\epsilon_{vj}\right]\chi_{vj}(r)=0 \tag{2}$$

is solved by expanding the rovibrational wave function $\chi_{vj}(r)$ in a Sturmian basis set. The full wave function is expanded in a set of channel functions $[n\equiv(vjl)]$,

$$\Psi^{JM}(\vec{R},\vec{r})=\frac{1}{R}\sum_n C_n(R)\phi_n(\hat{R},\vec{r}), \tag{3}$$

$$\phi_n(\hat{R},\vec{r})=\frac{1}{r}\chi_{vj}(r)\sum_{m_j}\sum_{m_l}(jlJ|m_j,M-m_l)Y^j_{m_j}(\hat{r})Y^l_{m_l}(\hat{R}), \tag{4}$$

where l is the orbital angular momentum of the atom with respect to the diatom, J is the total angular momentum, M is the projection of J onto the space-fixed z axis, and $(jlJ|m_j,M-m_l)$ denotes a Clebsch-Gordon coefficient. Operating the Hamiltonian (1) on the channel functions (3) leads to a set of coupled equations

$$\left[\frac{d^2}{dR^2}-\frac{l_m(l_m+1)}{R^2}+2\mu E_m\right]C_m(R)=\sum_n C_n(R)\times\langle\phi_m|U_I|\phi_n\rangle, \tag{5}$$

where E_m is the translational energy and l_m is the orbital angular momentum in the mth channel. The reduced interaction potential U_I is expanded in Legendre polynomials,

$$U_I(R,r,\theta)=2\mu V_I(R,r,\theta)=\sum_{\lambda=0}^{\infty}U_\lambda(R,r)P_\lambda(\cos\theta) \tag{6}$$

and the close-coupling equations (5) are solved using the general inelastic-scattering program MOLSCAT [23]. The cross sections and rate coefficients are given by [24]

$$\sigma_{vj\to v'j'}=\frac{\pi}{2\mu E_{vj}(2j+1)}\sum_{J=0}^{\infty}(2J+1)\times\sum_{l=|J-j|}^{|J+j|}\sum_{l'=|J-j'|}^{|J+j'|}|\delta_{jj'}\delta_{ll'}\delta_{vv'}-S^{J}_{jj'll'vv'}|^2, \tag{7}$$

$$R_{vj\to v'j'}(T)=(8k_BT/\pi\mu)^{1/2}\frac{1}{(k_BT)^2}\int_0^{\infty}\sigma_{v,j\to v',j'}(E_k)\times\exp(-E_k/k_BT)E_k dE_k, \tag{8}$$

where T is the temperature and k_B is Boltzmann's constant. In the present paper, we are mostly interested in the $T\to 0$ limit of Eq. (8). This asymptotic limit provides a good approximation for argon collisions with hydrogen molecules when the temperature is reduced to a few mK. The total quenching rate coefficients $R_{vj}(T)$ are given by

$$R_{vj}(T)=\sum_{v'j'}R_{vj\to v'j'}(T). \tag{9}$$

The complex scattering length $a_{vj}=\alpha_{vj}-i\beta_{vj}$ may be defined in terms of the quantities given in Eqs. (7)–(9) using the zero-energy elastic-scattering cross section

$$\sigma_{v,j\to v,j}=4\pi(\alpha_{vj}^2+\beta_{vj}^2)\approx 4\pi\alpha_{vj}^2 \tag{10}$$

and

$$\lim_{T\to 0}R_{vj}(T)=\frac{4\pi\hbar\beta_{vj}}{\mu}. \tag{11}$$

To obtain the predissociation lifetimes, the close-coupling equations are solved for energies below threshold, the S matrix is diagonalized and the eigenphase sum is differentiated with respect to energy to obtain numerically exact resonance widths. The predissociation lifetime is then given by $\tau_{vj,n}=\hbar/\Gamma_{vj,n}$ where n is the quantum number of the bound state of the van der Waals complex. The inverse of the predissociation lifetime of the most weakly bound state of the van der Waals complex was found to be well approximated by [2]

$$\tau_{vj}^{-1}=\frac{1}{2\pi r_{vj}|a_{vj}|^2}\left\{\left[1-\frac{2\alpha_{vj}r_{vj}}{|a_{vj}|^2}\right]^{-1/2}-1\right\}\lim_{T\to 0}R_{vj}(T), \tag{12}$$

where r_{vj} is the effective range for the channel potential labeled by v and j.

IV. MODEL

In many cases, we are only interested in bulk properties such as the total inelastic cross section or rate coefficient. In such cases, we would like to replace the exact coupled-channel formulation by an approximate optical potential model [25,26]. We consider the partial-wave Schrödinger equation

$$\left[\frac{1}{2\mu}\frac{d^2}{dR^2}-\frac{l(l+1)}{2\mu R^2}-V(R)+E\right]u_l(R)=0, \tag{13}$$

where $V(R)$ is a radially symmetric complex potential. In general, the imaginary part of the complex potential would depend on energy [25–27]. However, because the imaginary part of the scattering length is independent of energy, we may assume the complex potential is also energy independent in the $T\to 0$ limit. A simple model may be found by considering a complex square-well potential

$$U(R)=2\mu V(R)=\begin{cases}-(U_1+iU_2), & R<a,\\ 0, & R>a,\end{cases} \tag{14}$$

where U_1 and U_2 are real and $U_2\ll U_1$. The complex phase shift δ_0 is obtained in the usual way [28] by matching the interior and exterior radial functions and their derivatives at $R=a$. The result is

$$\delta_0=n\pi-ka\left(1-\frac{\tan\kappa a}{\kappa a}\right), \tag{15}$$

where $\kappa^2=k^2+U_1+iU_2$ and n is the number of bound states supported by the potential. The complex scattering length is

$$\alpha-i\beta=a\left(1-\frac{\tan\lambda a}{\lambda a}\right), \tag{16}$$

where

$$\lambda=\sqrt{U_1+iU_2}\approx\lambda_1+i\lambda_2 \tag{17}$$

with $\lambda_1=\sqrt{U_1}$ and $\lambda_2=U_2/2\sqrt{U_1}$. A connection to bound states may be made by performing a similar matching procedure with an exponentially decaying exterior function. For a weakly bound state with energy E and decay width Γ, the result is

$$\frac{\tan\lambda a}{\lambda}=-\left[2\mu\left(E-\frac{i}{2}\Gamma\right)\right]^{-1/2}. \tag{18}$$

Equations (16) and (18) lead to

$$E=\frac{-\hbar^2}{2\mu\alpha^2}\quad\text{and}\quad\Gamma=\frac{2\hbar^2\beta}{\mu\alpha^3}, \tag{19}$$

which agree with results derived previously [20]. Matching real and imaginary components in Eq. (16) yields

$$\alpha = a - \frac{\lambda_1 \tan(\lambda_1 a)\ \operatorname{sech}^2(\lambda_2 a) + \lambda_2 \tanh(\lambda_2 a)\ \sec^2(\lambda_1 a)}{(\lambda_1^2+\lambda_2^2)[1+\tan^2(\lambda_1 a)\tanh^2(\lambda_2 a)]}, \tag{20}$$

$$\beta = \frac{\lambda_1 \tanh(\lambda_2 a)\sec^2(\lambda_1 a) - \lambda_2 \tan(\lambda_1 a)\operatorname{sech}^2(\lambda_2 a)}{(\lambda_1^2+\lambda_2^2)[1+\tan^2(\lambda_1 a)\tanh^2(\lambda_2 a)]}. \tag{21}$$

Since we are interested in modeling inelastic collisions for weakly coupled systems, it is sufficient to consider potentials that satisfy the condition

$$\lambda_2 a \ll \cot \lambda_1 a. \tag{22}$$

Equations (20) and (21) may be simplified by using the leading order small-x approximations for the hyperbolic functions with $x=\lambda_2 a$. The result is

$$\alpha = a - \frac{\tan(\lambda_1 a)}{\lambda_1}, \tag{23}$$

$$\beta = \frac{\lambda_2}{\lambda_1}\left[a \sec^2(\lambda_1 a) - \frac{\tan(\lambda_1 a)}{\lambda_1}\right]. \tag{24}$$

In the following section, we show that the dimensionless ratio β/α obtained by solving the set of coupled equations (5) is not very sensitive to the details of the potential-energy surface. The complex square-well potential model provides a simple explanation for this behavior. Using Eqs. (23) and (24), we obtain

$$\frac{\beta}{\alpha} = \frac{U_2}{2U_1}[1+f(a\lambda_1)], \tag{25}$$

where

$$f(x) = \frac{x\tan^2 x}{x - \tan x}. \tag{26}$$

The function $f(x)$ has singularities at $x=(n+1/2)\pi$. These singularities are the so-called zero-energy resonances that occur when the nth bound state is located at exactly zero energy. Away from these singularities, it is useful to let $x = n\pi + \theta$ with the result

$$f(n\pi+\theta) = \frac{(n\pi+\theta)\tan^2\theta}{n\pi+\theta-\tan\theta}, \quad |\theta| < \pi/2. \tag{27}$$

Equation (27) is plotted in Fig. 3 for $n=0,1$, and 2. The figure shows that $f(n\pi+\theta)$ is flat and near zero for most of the allowed values of θ. Therefore, the ratio of imaginary to real part of the scattering length [see Eq. (25)] will be approximately equal to one half the ratio of imaginary to real part of the potential. Any linear variation in the reduced potential will scale out of the problem whenever θ is not too close to the singular end points. In this case, we would not expect the ratio of β to α to be very sensitive to the details of the potential. However, anomalous behavior may occur when θ is near one of the end points. In particular, the right side of the interval shows that for $n>0$ the function f has one additional singularity before reaching the end point corresponding to the zero-energy resonance. Equations (23)–(27) show that this additional singularity occurs when $\alpha=0$ and $\beta = \frac{1}{2}U_2 a^3$. This type of singularity is found in the scattering data for $Ar+H_2$ (see following section) but not for $He+H_2$ that supports only a single bound level. In order to analyze the end-point zero-energy resonance, it is convenient to use the result

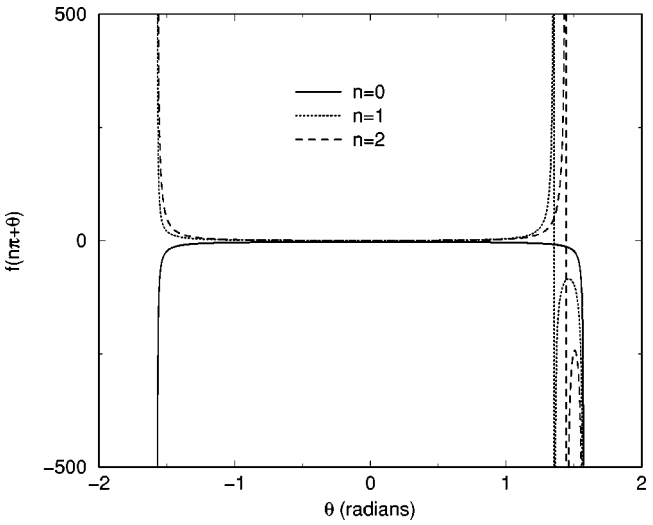

FIG. 3. The function $f(n\pi+\theta)$ as a function of θ for $n=0,1$, and 2.

$$\alpha = \frac{a}{[(n+1/2)\pi]^2}\ f[(n+1/2)\pi+\epsilon], \tag{28}$$

$$\beta = \left(\frac{a}{2}\right)\left(\frac{U_2}{U_1}\right)\left\{\frac{f[(n+1/2)\pi+\epsilon]}{(n+1/2)\pi}\right\}^2, \tag{29}$$

where

$$f[(n+1/2)\pi+\epsilon] = \frac{(n+1/2)\pi}{\epsilon}, \quad \epsilon \to 0. \tag{30}$$

It was found previously [21] that the ratio β/α^2 is a smooth function of the reduced mass in the vicinity of a zero-energy resonance. The complex square-well potential model provides a simple explanation for this behavior. The parameter ϵ in Eq. (30) is proportional to the reduced mass that is assumed to be a continuous variable. The components α and β diverge as $\epsilon \to 0$, but the ratio β/α^2 remains finite and is given by

$$\frac{\beta}{\alpha^2} = \frac{U_2}{U_1}\frac{[(n+1/2)\pi]^2}{2a}. \tag{31}$$

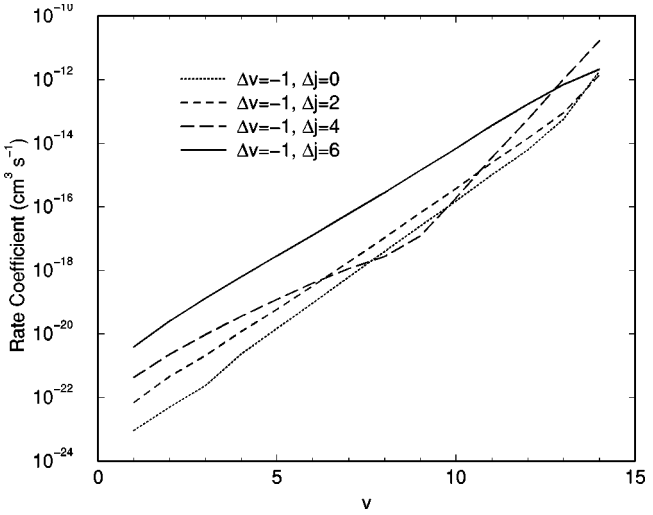

FIG. 4. Quantum-mechanical calculations of ultracold quenching rate coefficients for $Ar+H_2(v,j=0)$ as a function of the initial vibrational quantum number v. The calculations were performed using surface 2.

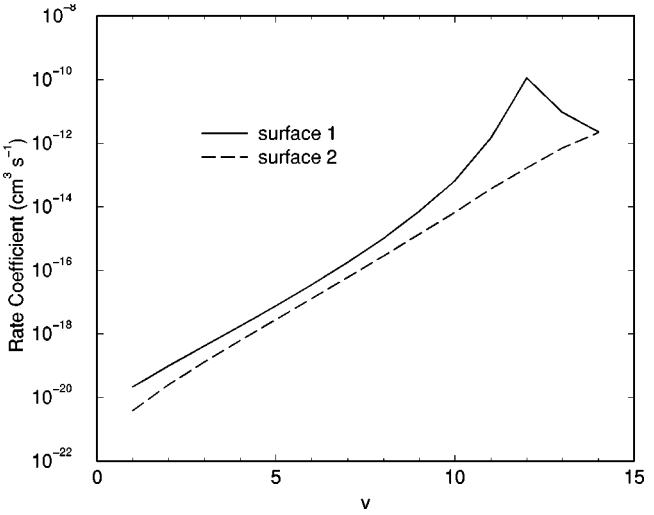

FIG. 5. Quantum-mechanical calculations of ultracold quenching rate coefficients for $Ar+H_2(v,j=0)$ as a function of the initial vibrational quantum number v. Both curves are for the $\Delta v=-1,\Delta j=6$ transition.

V. RESULTS

Figure 4 shows ultracold quenching rate coefficients for $Ar+H_2(v,j=0)$. These results were obtained by solving the close-coupling equations using surface 2. The $\Delta v=-1,\Delta j=6$ transition dominates all the others for $v<13$. Qualitatively similar behavior is found for surface 1. The specificity of this transition is reminiscent of the quasiresonant transitions that were found in $He+H_2(v,j)$ collisions in the limit of zero temperature [3,5,21]. In these transitions, the zero-temperature quenching rate coefficients are greatly suppressed at the value of j where the classical dynamics predicts there should be a maximum. The rate coefficients, however, tend to be greatly enhanced on either side of the classical peaks [3,5,21]. For H_2 molecules, the classical dynamics predicts a $\Delta v=-1,\Delta j=6$ peak at $j=6$ and a $\Delta v=-1,\Delta j=8$ peak at $j=4$. Because the $\Delta v=-1,\Delta j=8$ channels are either closed or very close to being closed, it is the $\Delta v=-1,\Delta j=6$ transition that dominates.

Figure 5 compares the ultracold rate coefficients for the dominant $\Delta v=-1,\Delta j=6$ transition computed using surface 1 with those computed using surface 2. The results differ by an order of magnitude or more for the two potential-energy surfaces and there is a strong maximum in the rate coefficient for surface 1 when $v=12$. As described in Sec. IV, the ratio of imaginary to real part of the complex scattering length provides a dimensionless parameter that is less sensitive to the choice of potential-energy surface. This is shown in Fig. 6. As expected, the two curves differ significantly near $v=12$. We investigated the anomalous behavior for surface 1 when $v=12$. Figure 7 shows the quenching rate coefficients as a function of the reduced mass. There is a strong maximum in the rate coefficients when the reduced mass is very close to its true value of 1.92 amu. Therefore, the anomalous behavior is due to a zero-energy resonance that occurs when the last bound state of the $Ar+H_2$ complex is pushed across the threshold. This feature is absent in the $v=12$, $j=0$ cross sections obtained using surface 2. However, we have found similar anomalous behavior for other values of v and j. Generally, such features are extremely sensitive to the fine details of the potential-energy surface.

The nearly exponential increase in the zero-temperature quenching rate coefficients as a function of vibrational quantum number is a consequence of the energy mismatch between the initial and final diatomic states. In Fig. 8 we plot the dominant $\Delta v=-1,\Delta j=6$ transition vs the final momentum for the $j=0$ initial state. The $v=1$ rate coefficient is at the far right of each curve with the higher v's moving leftward in ascending order. Because these transitions are quasiresonant, the indirect coupling terms are important [21,29] and the rate coefficients deviate from the exponential momentum-gap dependence that is often found in vibrational predissociation [30]. Figure 8 shows that the rate coefficients

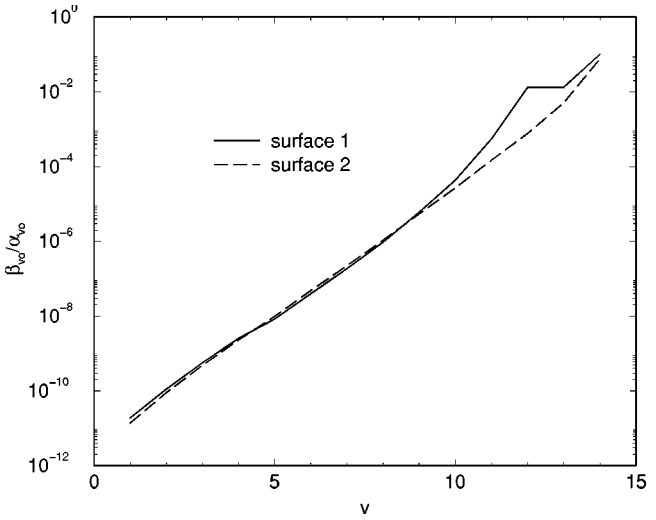

FIG. 6. Ratio of α_{v0} to β_{v0} as a function of the initial vibrational quantum number v.

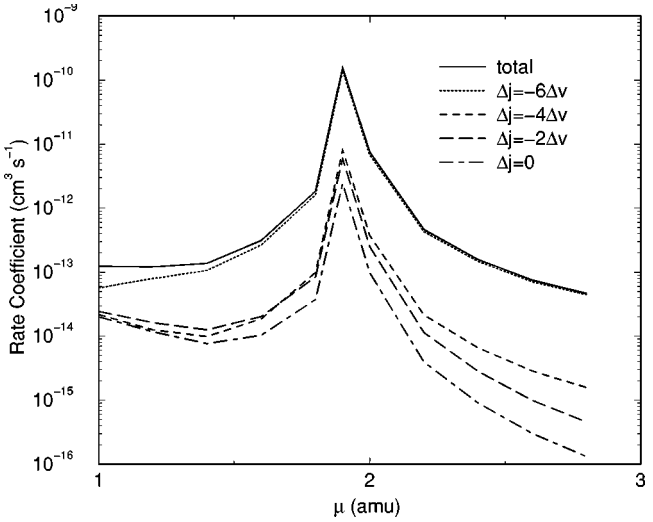

FIG. 7. Rate coefficients for the $v=12,j=0$ initial state as a function of the reduced mass μ. The total quenching rate coefficient is dominated by the $\Delta v=-1,\Delta j=6$ contribution and has a peak very close to the physical reduced mass of 1.92 amu. Surface 1 was used for these calculations.

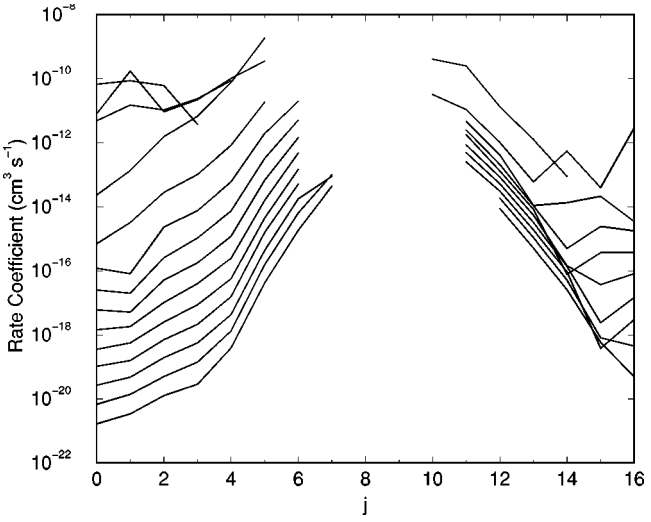

FIG. 9. Rate coefficients for the $\Delta j=-4\Delta v$ transition as a function of the initial rotational quantum number j. The curves increase vertically with increasing vibrational quantum number v starting with $v=1$. The gap in the center of the curves is due to the closing of the $\Delta j=-4\Delta v$ transition. Surface 1 was used for these calculations. Irregular behavior begins to appear when $v\geqslant 12$.

deviate more strongly from the exponential momentum-gap behavior as the vibrational quantum number is increased. This is to be expected considering that the rate coefficients must tend to zero as the momentum gap is closed [21].

Rotational distributions of zero-temperature inelastic quenching rate coefficients are shown in Figs. 9 and 10 for $\Delta j=-4\Delta v$ transitions. The curves increase vertically with increasing vibrational quantum number v starting with $v=1$. The gap in the center of the curves is due to the closing of the transition. To the left of the gap, it is the $\Delta v=-1,\Delta j=4$ transition that is open, whereas to the right of the gap, it is the $\Delta v=1,\Delta j=-4$ transition that is open. These curves are similar to those reported previously for HeH_2 [3,21]. However, because the ArH_2 surfaces allow for greater diatomic stretching, we have included the rate coefficients for high values of v. It is interesting to note that irregular behavior appears in both sets of calculations, but at different values of v. We believe this irregular behavior is related to the decreasing energy difference between the van der Waals potential well and the diatomic energy spacings as v increases. Because the potential wells are deeper for surface 2 than surface 1, it is not surprising that the irregular behavior

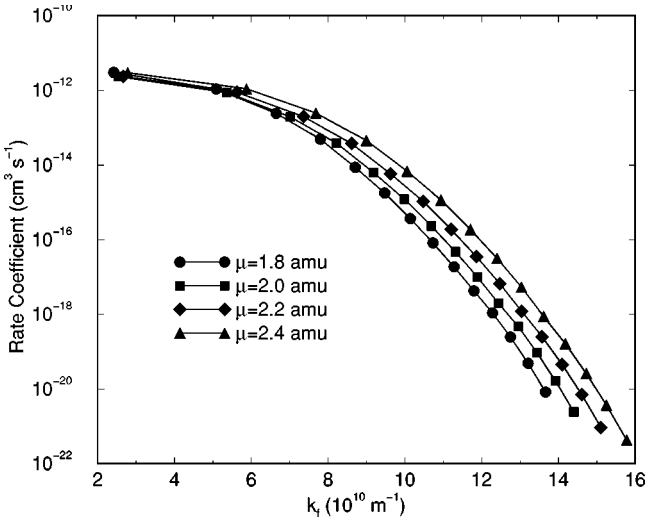

FIG. 8. Rate coefficients for the $\Delta v=-1,\Delta j=6$ transition as a function of the final momentum k_f and reduced mass μ. For each curve, the low vibrational levels are at the far right and the high vibrational levels are at the far left, and the rotational level is zero. Surface 2 was used for these calculations.

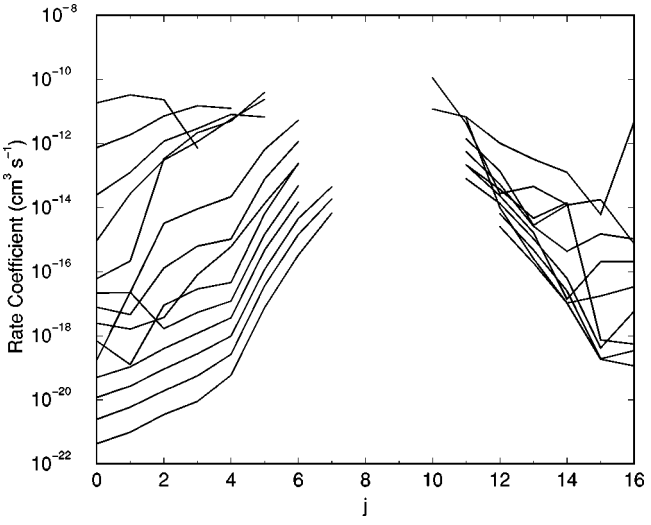

FIG. 10. Rate coefficients for the $\Delta j=-4\Delta v$ transition as a function of the initial rotational quantum number j. The curves increase vertically with increasing vibrational quantum number v starting with $v=1$. The gap in the center of the curves is due to the closing of the $\Delta j=-4\Delta v$ transition. Surface 2 was used for these calculations. Irregular behavior begins to appear when $v\geqslant 5$.

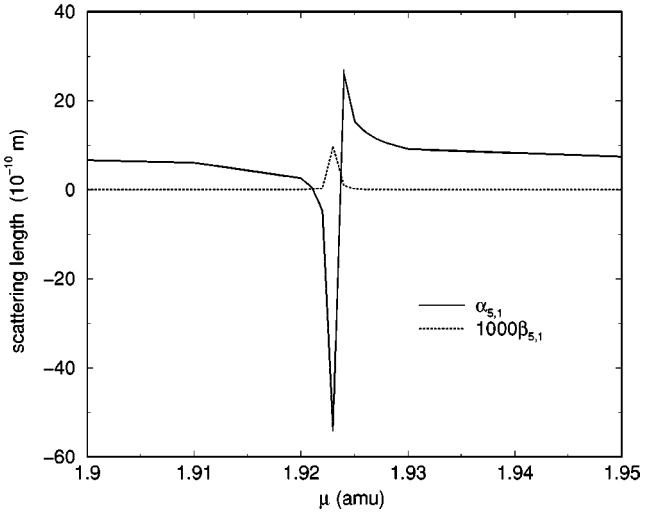

FIG. 11. Real and imaginary components of the complex scattering length for $v=5, j=1$ as a function of the reduced mass. Surface 2 was used for these calculations. The value of $\alpha_{5,1}$ varies between 5 and $-\infty$ in the vicinity of the physical reduced mass of 1.92 amu. The value of $\beta_{5,1}$ has been multiplied by a factor of 1000 in order to be seen on the same graph.

for the surface 2 results begin at smaller values of v compared to the surface 1 results.

We studied the irregular behavior of the rate coefficient for the $v=5, j=1$ level calculated using surface 2 (see Fig. 10). The real and imaginary components of the complex scattering length are plotted in Fig. 11 as a function of the reduced mass. The imaginary part $\beta_{5,1}$ has been multiplied by a factor of 1000 in order to be seen on the same graph. Figure 11 shows that the value of $\alpha_{5,1}$ passes through zero in the vicinity of the physical reduced mass of 1.92 amu. As described in Sec. IV, this behavior can only occur for systems that have at least one bound state in addition to the state corresponding to the zero-energy resonance. When μ is tuned to the zero-energy resonance, the values of $\alpha_{5,1}$ and $\beta_{5,1}$ show behavior similar to Eqs. (28) and (29) derived for a complex square-well potential. It is interesting to note that the zero-temperature rate coefficients for $He+H_2$ [21] did not show the kind of irregular behavior seen here because the $He\cdots H_2$ van der Waals complex only supported one bound state for each rovibrational level. When the reduced mass was varied in order to move this bound state into a zero-energy resonance [21], then the system behaved similar to the $n=0$ curve shown in Fig. 3 and it was not possible for α to pass through zero.

Recent calculations [21] used effective range theory to study the effect of quasiresonant dynamics on the predissociation of the most weakly bound states of van der Waals molecules. The distribution of predissociation lifetimes with initial diatomic rotational quantum number revealed interesting structure that was interpreted using classical dynamics. Figure 12 shows a similar distribution for $Ar+H_2(v,j)$ for $j<10$. These results were obtained for the highest vibrational level of the $l=0$ van der Waals complex using the eigenphase sum method [2]. The similarity between these distributions supports the reliability of the effective range theory

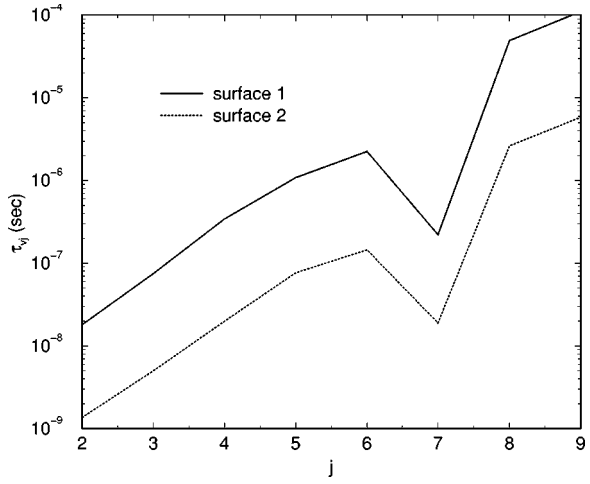

FIG. 12. Predissociation lifetime of the most weakly bound state of the $Ar\cdots H_2(v,j)$ complex for $v=2$ as a function of j. The solid curve was computed using surface 1 and the dotted curve was computed using surface 2.

for the most weakly bound state. Figure 13 shows that the rotational distribution for less weakly bound states of the complex also possess the same qualitative structure. This suggests that classical dynamics is playing a role for these states as well.

VI. CONCLUSIONS

We have investigated cold collisions using two different parametrizations of the electronic potential-energy surface for argon atoms interacting with hydrogen molecules [17]. By comparing the results of these two sets of calculations, we estimate that our scattering data is reliable to within an order of magnitude when there is no anomalous threshold behavior. The ratio of real to imaginary part of the scattering length is not as sensitive to the potential energy surface and is typically reliable to within a factor of 2. Because surface 2

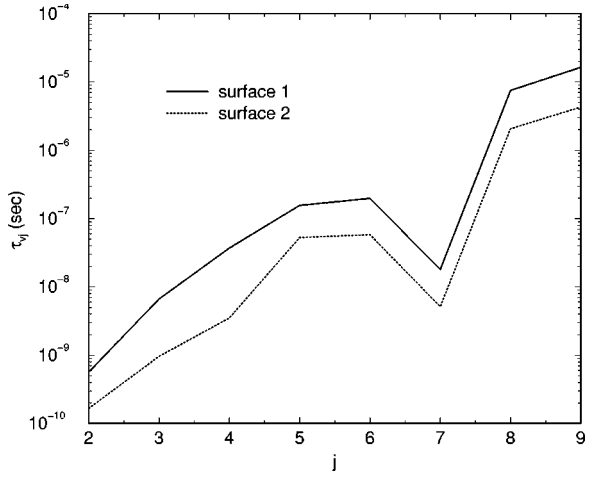

FIG. 13. Predissociation lifetime of the second most weakly bound state of the $Ar\cdots H_2(v,j)$ complex for $v=2$ as a function of j. The solid curve was computed using surface 1 and the dotted curve was computed using surface 2.

does a better job of reproducing the van der Waals well [17], we believe the results obtained using surface 2 are probably more reliable than those obtained using surface 1.

We have shown that a simple complex square-well potential model is very useful for interpreting the results of complicated coupled-channel calculations. For weakly coupled systems, the ratio of real to imaginary part of the scattering length is typically equal to twice the ratio of real to imaginary part of the square-well potential when there is no anomalous threshold behavior present. The radius of the square-well potential may be used as an additional fitting parameter for cases where anomalous threshold behavior exists.

Both sets of scattering data reveal resonant and quasiresonant behavior. As expected, the resonances are very sensitive to the details of the surface, so predictions of the resonant parameters are not quantitatively reliable. However, the qualitative features of the resonant and quasiresonant behavior are similar for both sets of scattering data. Therefore, we would expect that new data obtained from trapped molecule experiments could be readily used to select and fine tune the potential-energy surface.

ACKNOWLEDGMENTS

We would like to thank D. Schwenke for providing us with a computer program for computing the potential-energy surfaces. This work was funded by the National Science Foundation through Grant No. PHY-0070920. The initial stages of the research were also funded by the NSF through a grant for the Institute for Theoretical Atomic and Molecular Physics at Harvard University and Smithsonian Astrophysical Observatory.

[1] N. Balakrishnan, R. C. Forrey, and A. Dalgarno, Phys. Rev. Lett. **80**, 3224 (1998).

[2] R. C. Forrey, V. Kharchenko, N. Balakrishnan, and A. Dalgarno, Phys. Rev. A **59**, 1 (1999); R. C. Forrey, N. Balakrishnan, V. Kharchenko, and A. Dalgarno, *ibid.* **58**, R2645 (1998).

[3] R. C. Forrey, N. Balakrishnan, A. Dalgarno, M. Haggerty, and E. J. Heller, Phys. Rev. Lett. **82**, 2657 (1999).

[4] N. Balakrishnan, A. Dalgarno, and R. C. Forrey, J. Chem. Phys. **113**, 621 (2000).

[5] R. C. Forrey, Phys. Rev. A **63**, 051403(R) (2001).

[6] J. D. Weinstein, R. deCarvalho, T. Guillet, B. Friedrich, and J. M. Doyle, Nature (London) **395**, 148 (1998); J. Doyle and B. Friedrich, Chem Br. **35**, 31 (1999).

[7] F. Stienkemeier, W. E. Ernst, J. Higgins, and G. Scoles, J. Chem. Phys. **102**, 615 (1995); J. Higgins, C. Callegari, J. Reho, F. Stienkemeier, W. E. Ernst, K. K. Lehmann, M. Gutowski, and G. Scoles, Science **273**, 629 (1996).

[8] A. Fioretti, D. Comparat, A. Crubellier, O. Dulieu, F. Masnou-Seeuws, and P. Pillet, Phys. Rev. Lett. **80**, 4402 (1998).

[9] A. N. Nikolov, J. R. Ensher, E. E. Eyler, H. Wang, W. C. Stwalley, and P. L. Gould, Phys. Rev. Lett. **84**, 246 (2000); A. N. Nikolov, E. E. Eyler, X. Wang, H. Wang, J. Li, W. C. Stwalley, and P. L. Gould, *ibid.* **82**, 703 (1999).

[10] T. Takekoshi, B. M. Patterson, and R. J. Knize, Phys. Rev. A **59**, R5 (1999); T. Takekoshi, B. M. Patterson, and R. J. Knize, Phys. Rev. Lett. **81**, 5109 (1998).

[11] J. M. Gerton, D. V. Strekalov, I. D. Prodan, and R. G. Hulet, Nature (London) **408**, 692 (2000).

[12] R. Wynar, R. S. Freeland, D. J. Han, C. Ryu, and D. Heinzen, Science **287**, 1016 (2000).

[13] H. L. Bethlem, G. Berden, and G. Meijer, Phys. Rev. Lett. **83**, 1558 (1999); H. L. Bethlem, G. Berden, A. A. van Roij, F. M. H. Crompvoets, and G. Meijer, *ibid.* **84**, 5744 (1999).

[14] M. Gupta and D. Herschbach, J. Phys. Chem. A **103**, 10 670 (1999).

[15] J. A. Maddi, T. P. Dinneen, and H. Gould, Phys. Rev. A **60**, 3882 (1999).

[16] C. J. Williams and P. S. Julienne, Science **287**, 986 (2000).

[17] D. W. Schwenke, S. P. Walch, and P. R. Taylor, J. Chem. Phys. **98**, 4738 (1993).

[18] F. Legare, S. Chelkowski, and A. D. Bandrauk, Chem. Phys. Lett. **329**, 469 (2000).

[19] D. M. Villeneuve, S. A. Aseyev, P. Dietrich, M. Spanner, M. Yu. Ivanov, and P. B. Corkum, Phys. Rev. Lett. **85**, 542 (2000).

[20] N. Balakrishnan, V. Kharchenko, R. C. Forrey, and A. Dalgarno, Chem. Phys. Lett. **280**, 5 (1997).

[21] R. C. Forrey, N. Balakrishnan, A. Dalgarno, M. Haggerty, and E. J. Heller, Phys. Rev. A **64**, 022706 (2001).

[22] B. Stewart, P. D. Magill, T. P. Scott, J. Derouard, and D. E. Pritchard, Phys. Rev. Lett. **60**, 282 (1988); P. D. Magill, B. Stewart, N. Smith, and D. E. Pritchard, *ibid.* **60**, 1943 (1988).

[23] J. M. Hutson and S. Green, MOLSCAT computer code, version 14 (1994), distributed by Collaborative Computational Project No. 6 of the Engineering and Physical Sciences Research Council (UK).

[24] A. M. Arthurs and A. Dalgarno, Proc. R. Soc. London, Ser. A **256**, 540 (1963).

[25] M. H. Ross and G. L. Shaw, Ann. Phys. (N.Y.) **9**, 391 (1960).

[26] D. A. Micha, *Optical Models in Molecular Collision Theory*, Dynamics of Molecular Collisions Part A, edited by W. H. Miller (Plenum Press, New York, 1976).

[27] A. D. Bandrauk, E. E. Aubanel, and J.-M. Gauthier, *Theory of Molecules in Intense Laser Fields*, Molecules in Laser Fields, edited by A. D. Bandrauk (Marcel Dekker, New York, 1994).

[28] C. J. Joachain, *Quantum Collision Theory* (North-Holland, Amsterdam, 1975).

[29] J. M. Hutson, C. J. Ashton, and R. J. LeRoy, J. Chem. Phys. **87**, 2713 (1983); R. J. LeRoy, G. C. Corey, and J. M. Hutson, Faraday Discuss. Chem. Soc. **73**, 339 (1982).

[30] G. E. Ewing, Chem. Phys. **29**, 253 (1978); G. E. Ewing, *ibid.* **71**, 3143 (1979); G. Ewing, *ibid.* **72**, 2096 (1980).